Compact Dual-Layered Wideband Wearable Monopole Antenna with Circular Parasitic Element for Breast Cancer Detection

[1,2]Nur'Atika Binti Koma'rudin, [1]Zahriladha Zakaria, [1]Nornikman Hassan, [2]Mohd Manoj Jumidali, [3]Ping Jack Soh

[1]Microwave Research Group (MRG), Centre for Telecommunication Research & Innovation (CeTRI), Fakulti Kejuruteraan Elektronik dan Kejuruteraan Komputer (FKEKK) Universiti Teknikal Malaysia Melaka (UTeM) Hang Tuah Jaya, Durian Tunggal 76100, Malaysia.

[2]Advanced Technology Training Centre (ADTEC Melaka), Department of Human Resource, Ministry of Human Resource, Bandar Vendor Taboh Naning 78000 Alor Gajah Melaka, Malaysia.

[3]Centre for Wireless Communications (CWC), University of Oulu, 90014 Oulu, Finland.

***Abstract*— A dual-layered wideband antenna with coplanar waveguide (CPW)-base and circular parasitic element technique was proposed. In comparison to past research problems, which largely produced omnidirectional and hard antennas, it should be flexible, unidirectional, wideband, low weight, and compact. The wearable antenna consists of three stages, whereby Antenna *A* is designed by a basic rectangular antenna with CPW. Design B is the next stage of antenna design development with the patch size modified. Antenna *C* is the next development stage with extra circular parasitic element and felt substrate. The bandwidth of 4.11 GHz (79.8 %) of the proposed antenna, which ranges from 2.89 GHz to 7.0 GHz, combines a number of wideband resonant frequencies, including those at 3.07 GHz, 3.90 GHz, 4.35 GHz, 5.15 GHz, and 6.32 GHz. There is also a 40 MHz-wide narrowband that functions between 1.15 GHz and 1.19 GHz and with resonance at 1.17 GHz. This proposed antenna is designed to develop a multifunction application future work system, particularly for breast cancer detection.**

***Keywords*— Wearable antennas, ultrawideband antennas, unidirectional antennas, microwave imaging**

INTRODUCTION

Currently, new communication systems with low prices, simplicity, high data rates and efficiency will be required as the number of users increases [1]. in recent decades, increase in demand, particularly in the military and medical procedures which require tracking, monitoring, and screening, has resulted in significant advancements in microwaves and radio frequencies [2]. Cancer is described as the uncontrolled, fast growth and division of aberrant cells which experience alterations that disrupt their normal, orderly cellular life cycles. The most frequent cancer type diagnosed and the main cause of global cancer-related mortality in women is breast cancer [3]. Worldwide, breast cancer had claimed the lives of over 685,000 women in 2020 with nearly two-thirds of such fatalities happened in less developed areas [4]. At present the most effective methods for managing and treating breast cancer are breast screening and early diagnosis.

Microwave imaging (MWI) is garnering much interest as a possible diagnostic technique for early breast cancer detection amongst other imaging modalities, which are now used to identify breast cancer [5]. Due to its non-invasive, affordable, and non-ionisation qualities, MWI for cancer diagnosis has captured the interest of scientists and engineers for many years [6]. Breast cancer diagnosis is one of the most promising uses for MWI technology since it has potential to identify diseased tissue due to the dielectric characteristics differential which emerges between normal and malignant tissues [7]. During the past few decades, microwave imaging had evolved various signal processing methods (algorithms) as well as a set of antennas for these sorts of applications. These methods may generally be categorised as passive, active or hybrid methods.

The design of assess embedded or concealed in any material or structure by using electromagnetic (EM) waves (300 MHz – 300 GHz), microwave imaging is a cutting-edge scientific approach that has evolved from detecting or finding techniques (radar or tomography technique) [8]. Consequently, the cancer detection method in Malaysia is painful: magnetic resonance imaging (MRI) technology is restricted to large hospitals due to operational staff knowledge, high cost of procurements and size of equipment is too big [9]. X-rays emit ionising radiation, which may be dangerous for repeated exposure.

Antennas are major elements of the MWI system for transmitting and receiving radio frequency (RF) information [10]. In addition, a wideband response of an antenna was investigated with various specifications, including imaging frequency, physical size, material use, and design methodology. The key element of wireless sensing systems brought to the medical sector and applications is wearable antennas. The operation of wearable antennas is intended to be close to the human body. Due to the fact that these suggested antennas will establish contact with the human body, a thorough design strategy that takes wearability and a solid communication link into account is needed.

A wearable antenna must be pleasant for the user and flexible with body movements because it is practically worn on the patient's clothing. Wideband antenna designs are far more challenging than narrowband antenna designs. According to previous research, a wideband antenna may be produced by employing a circular patch, partial ground, addition of a parasitic element, construction of a stair at the edge of patch and a ground structure with flaws. Wide bandwidth may be easily achieved by utilising the circular monopole antenna designs, making them ideal for wideband applications like microwave imaging systems [12].

In Jan's research [13], a novel planar monopole antenna was presented, in which it was designed on a low loss FR4 substrate. The dimension of proposed antenna was 26 mm × 25 mm which was operated at frequency band of 3.2 GHz to 12 GHz [13]. The antenna performed with wideband response and stable radiation patterns with enhanced performance at peak gain of 4 dB. Hossain [14] presented a diamond-shaped patch for the resonator area that measured 29 mm by 24 mm by 1.5 mm; a parasitic resonator component with a four-sided form; a triple-octangular shape; and a limited ground plane slotting. With a working band of 2.80 GHz – 11.50 GHz, a respectable bandwidth of 8.7 GHz and an average efficiency of 75 %, the parasitic ring-shaped components improved the performance of antenna.

The greatest gain which this antenna could get was 5.80 dBi. In breast imaging usage, Cherian presented a thin antenna of dimension 28 mm x 35.5 mm which was constructed on FR4 substrate [15]. The antenna could identify tumours as tiny as 6 mm and operated between 3.74 GHz and 9.5 GHz. The suggested design of antenna was quite intricate, the substrate used was inappropriate for wearable applications and it produced a bi-directional pattern. Several studies that applied a directional radiator at the monopole antenna for MWI breast application were done [16–20]. It was discovered that (quasi)-omnidirectional radiating antennas were often the outcome of a wideband operation required for a better image resolution. Along with making the antenna construction bulkier and necessitating the integration of backings, this made the design more difficult. As back radiation reduced the effectiveness of MWI systems, unidirectional radiation increased antenna gain.

Therefore, this work proposes a compact dual-layered monopole antenna with a circular parasitic element. This dual-layered monopole antenna, together with the coplanar waveguide (CPW) feedline, allowed the antenna to produce unidirectional radiation with a broad operational bandwidth. Three design enhancement steps were considered, namely Antenna *A*, Antenna *B* and Antenna *C*.

ANTENNA DESIGN

The construction of the dual-layered monopole antenna had three distinct stages, commencing with antenna Design *A*, Design *B,* and Design *C*. This antenna was made up of a simulation component created in CST Microwave Studio and a laboratory-fabricated component. ShieldIT materials were employed to create the wearable antenna as conductors (electric conductivity = 1.1). The low resistance of this cloth was less than 0.1 / sq. Additionally, it showed that SheildIT was 0.17 mm thick as compared to the 2.0 mm thickness of substrate. The conducting portion of an antenna is thus mostly supported by the substrate materials to enhance the radiating characteristics. Felt has a dielectric constant of 1.45 and a tangent loss of 0.045 for electrical conductivity. By binding and compressing fibres together with the help of moisture and heat, this felt is a type of textile.

A. Antenna A

Figure 1 shows the schematic diagram of Antenna *A*. Initial design of Antenna *A1* was a basic rectangular microstrip patch antenna. The patch portion at the front of antenna enclosed this antenna. In addition, feedlines which were linked by using SMA connectors existed. It included the entire ground plane which used SheildIT in the rear. For breast imaging, a planar-type design is ideal because it allows the antenna to be placed directly on the target.

Due to the fundamental drawback of limited bandwidth of the microstrip patch antenna, the next design was created. As a result, Antenna *A2* showed the conversion of the ground plane to a co-planar waveguide at the bottom front patch of antenna. The CPW in this instance had a width of 10.0 mm and length of 8.3 mm. This CPW was able to increase the bandwidth of antenna. The side-plane conductor serves as ground, while the middle strip carries signal, which is fed by the CPW. The CPW fed slot antenna has the benefit of having wideband characteristics. As a consequence, the CPW fed slot antenna represents the most efficient and desirable antenna for wideband wireless applications.

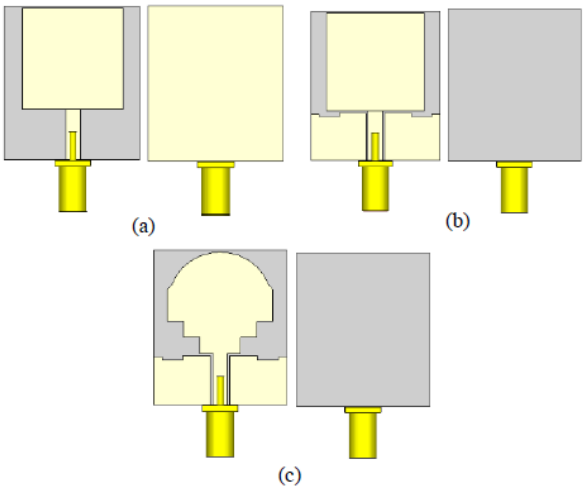

Fig. 1. Schematic diagram of Antenna A (front view and back view), (a) Antenna *A1*, (b) Antenna *A2*, (c) Antenna *A3*

B. Antenna B

Design B is the next development stage of the antenna design, with modification of patch size. Similar to Antenna *A1*, this antenna stage comprised the basic patch from SheildIT material that was located above of the felt substrate. It also comprehended a ground plane at the back of antenna. The difference is size of the antenna. For Antenna *B1*, the substrate dimension was 79.0 mm (length) x 69.0 mm (width). This patch was connected with a 39.0 mm (length) x 3.0 mm (width) feedline and the SMA conductor. It had co-planar waveguide of SheildIT material at the front part of antenna. Different from Antenna *B2*, it has an additional structure of a ground plane. A ground plane is a large-scale conducting surface, such as the Earth, which is connected to the ground line of transmitter and acts as a reflecting surface for signals. Figure 2 illustrates the schematic diagram of front view shape and side view for Antenna *B*.

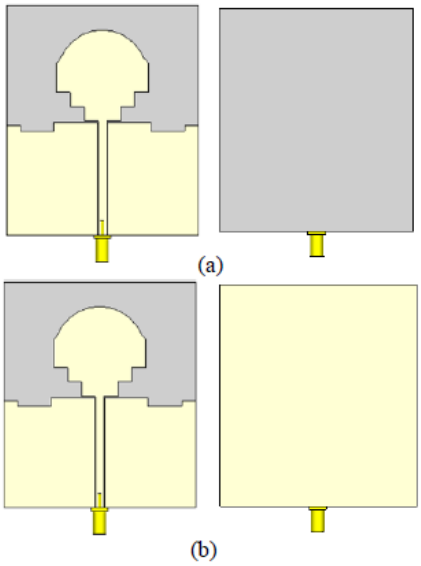

Fig. 2. Schematic diagram for Antenna *B* (front view and back view), (a) Antenna *B1*, (b) Antenna *B2*

C. Antenna C

Then, it goes to the improvement version of the antenna Design *B*. Figure 3 represents the proposed wideband wearable antenna of Design *C*. In this stage, the circular parasitic patch was connected to a microstrip line, which was located on the next layer, followed by substrate Layer 2 (also felt). To observe the change in the return-loss parameter, a circular patch was developed instead of a rectangular patch. This circular parasitic patch has capability to improve the forward directivity of antenna. Finally, a full ground plane completes this antenna at the bottom layer by using ShieldIT.

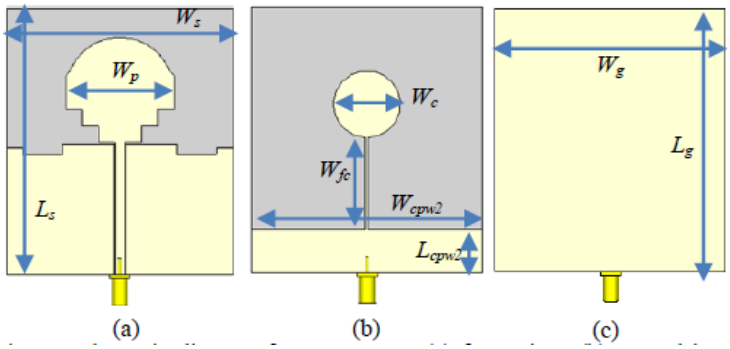

Fig. 3. Schematic diagram for Antenna *C*, (a) front view, (b) second layer and (c) back view

The overall antenna (and substrate) size was dimensioned at 79 mm (substrate length, L_s) × 69 mm (substrate width, W_s). The CPW line which feeds the main patch was sized at 39 mm (length, L_{f1}) × 3.0 mm (width, W_{f1}), and terminated with a SubMiniature Version A (SMA) connector. On the other hand, the rectangular section of the parasitic patch located on substrate Layer 2 was dimensioned at 69.0 mm (length, L_{cpw2}) × 13.0 mm (width, W_{cpw2}), whereas the feedline connecting this patch to the circular patch was 27.0 mm (length, L_{fc}) × 0.5 mm (width, W_{fc}). The diameter of the circular patch, W_c was 26.0 mm.

RESULT

A. Antenna A

Antenna *A1*, Antenna *A2*, and Antenna *A3*'s return loss and resonant frequency point are displayed in Figure 4 and Table 1. Original design of Antenna *A1* resonates between a number of frequencies that are close to 6.53 GHz. It displays simulation results with lower frequency, f_{Low}, higher frequency, f_{High}, and resonant frequency, f_r, values at 6.29 GHz and 6.75 GHz for the resonant frequency of 6.53 GHz. At this time, it displays a return loss of – 37.73 dB.

This is the standard behaviour of the fundamental rectangular antenna with narrow band effect. This antenna has a 0.46 GHz bandwidth. In another FBR outcome situation, the Antenna *A1* has a front main lobe magnitude direction of + 3.5 dB at 00 and a rear lobe magnitude direction of - 4.86 dB at 180^0. In this instance, the front-to-back ratio of antenna is 8.36 dB at a resonance frequency of 6.53 GHz.

Then, the ground plane transitions from the standard ground at rear of antenna into the co-planar waveguide types. The design of Antenna *A2* will have an impact on where its resonance frequency is located. The resonant frequency in this instance was changed from 6.53 GHz to 3.82 GHz, which was a lower frequency. Additionally, it lowers the return loss performance to just - 11.32 dB. The bandwidth now covers the frequency range of 3.48 GHz to 4.28 GHz, increasing its range to 0.79 GHz from 0.46 GHz. The front main lobe magnitude direction for Antenna *A2* FBR result was + 1.81 dB at 0°, while the rear lobe magnitude direction was - 1.91 dB at 180°. For a resonance frequency of 3.82 GHz, the front-to-back ratio of antenna in this instance was 3.27 dB.

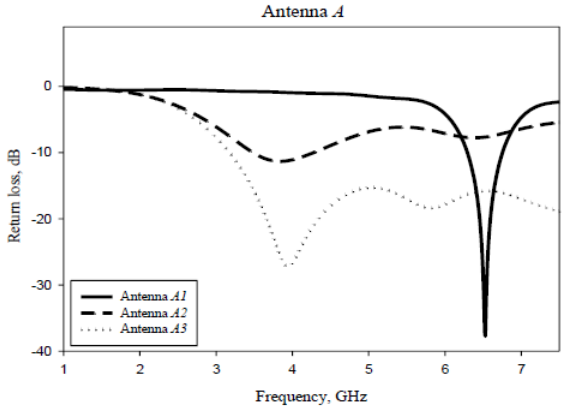

Fig. 4. Return loss of Antenna *A*

Next, the final antenna design,which was Antenna *A3*, with a modified patch antenna design, was presented. The improvements have a substantial impact on bandwidth. In this instance, the co-planar waveguide with 3.82 GHz has a broad influence on the bandwidth, starting at 3.17 GHz and going all the way up to 7.50 GHz. It demonstrates that the resonant frequency is 3.94 GHz with a return loss of - 27.18 dB. At the resonance frequency of 3.94 GHz, the FBR of this antenna is 4.21 dB. The primary lobe of antenna in the forward direction measures 2.14 dB, while the rear lobe is at - 2.07 dB.

The gain and directivity characteristics of Antenna *A1* were found to be 4.27 dB and 7.62 dBi, respectively. However, at the initial resonance frequency, the gain and directivity performance of Antenna *A2* were reduced to just 1.98 dB and 2.69 dBi, respectively. The gain and directivity performance for the second resonant frequency were 2.43 dB and 3.32 dBi, respectively. This circumstance was a result of the ground plane being translated into the co-planar waveguide technology. However, as compared to Antenna *A3*, it is boosting gain performance again by 2.20 dB, which has the unintended consequence of further decreasing directivity to just 2.29 dBi for the initial resonant frequency.

TABLE I. DIFFERENT PERFORMANCE RESULTS OF ANTENNA *A*

Ant	Resonant frequency, f_r (GHz)	Return loss (dB)	Bandwidth (GHz), $f_{High} - f_{Low}$ (GHz)	Gain (dB)	Dircv (dBi)	FBR (dB)
A1	6.53	- 37.73	0.46, 6.29 – 6.75	4.27	7.62	8.36
A2	3.82	- 11.32	0.79, 3.48 – 4.28	1.94	2.69	3.72
	6.68	- 12.36	0.81 6.19 -7.00	2.43	3.32	3.45
A3	3.94	- 27.18	3.82, 3.17 – 7.50	2.20	2.29	4.21
	5.81	- 18.84		2.89	3.58	4.23

B. Antenna B

The adjustable size of Antenna *B* continued to go through the development stage. Antenna *B1* and Antenna *B2* were the two stages being considered in this section. Co-planar waveguide built of SheildIT material was located at the front of Antenna *B1*. The ground plane construction sets it apart from Antenna *B2*. The return loss of Antenna *B1* and Antenna *B2* is depicted in Figure 5. The varied findings for parameters for two distinct performances of Antenna *B* are shown in Table 2.

Resonance frequencies of Antenna *B1* were 1.90 GHz and 5.62 GHz, respectively, with return loss performances of – 37.02 dB and – 19.50 dB. The same applies to Antenna B2, which resonates at two separate points in frequency. It resonates at 3.27 GHz with – 19.58 dB at the first site, and at 5.18 GHz with – 28.06 dB resonance at the second location. The initial resonant frequency for Antenna *B1* ranges from 1.48 GHz to 3.73 GHz, with a bandwidth of 2.25 GHz.

In the other section, the second resonant frequency resonates between 4.61 GHz and 7.15 GHz in frequency range and has a bandwidth of 2.54 GHz. Meanwhile, the first and second resonant frequencies at 3.27 GHz and 5.18 GHz, respectively, revealed the reduced value of bandwidth with just 0.22 GHz and 0.77 GHz, respectively, for the Antenna *B2* device. This resulted from the ground plane being added to the rear of antenna.

In another finding, it was found that gain performance of this antenna for the first and second resonant frequencies was 2.13 dB and 3.98 dB, respectively. It demonstrated that first and second resonant frequencies of Antenna *B2*, respectively, were 2.49 dB and 1.68 dB. With a forward loop of 0° and 180° and an initial resonant frequency of 1.90 GHz, FBR of Antenna *B1* was 5.37 dB. It has an FBR of 5.40 dB at a different resonant frequency of 5.62 GHz.

Initial resonance frequency of Antenna *B2* was 3.27 GHz, with an equal front and back lobe magnitude and FBR of 10.36 dB at 0° and 180°, respectively. With the second resonant frequency of 5.18 GHz, this was different. It contained two front lobes which were approximately equal in size, 135° and 235°, and a rear loop with a maximum point at 7.58 dB and a forward loop that was 30° and 330°. With 12.43 dB of FBR, it had the highest FBR.

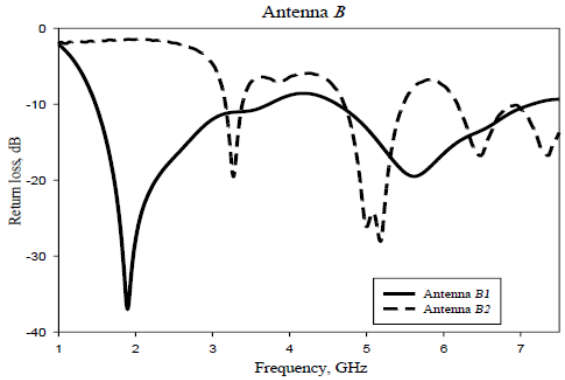

Fig. 5. Return loss of Antenna *B*

TABLE II. DIFFERENT PERFORMANCE RESULTS OF ANTENNA *B*

Ant	Resonant frequency, f_r (GHz)	Return loss (dB)	Bandwidth (GHz), $f_{High} - f_{Low}$ (GHz)	Gain (dB)	Dircv (dBi)	FBR (dB)
B1	1.90	– 37.02	2.25, 1.48 – 3.73	2.13	2.85	5.37
	5.62	– 19.50	2.54, 4.61 – 7.15	2.15	3.98	5.40
B2	3.27	– 19.58	0.22, 3.17 – 3.39	2.49	8.43	10.36
	5.18	– 28.06	0.77, 4.70 – 5.48	1.68	7.61	12.43

C. Antenna C

Antenna *C* was the following development stage procedure. The extra circular parasitic element and felt substrate made up the planned Antenna *C*. The substrate was 69.0 mm of width and 79.0 mm of length. The patch was connected to a SMA conductor and a feedline that was 39.0 mm long and 3.0 mm wide. The feedline of the proposed antenna connects the second layer of the circular patch construction to the CPW structure below the antenna.

The bandwidth of this antenna, which ranged from 2.89 GHz to 7.0 GHz, was greater than that of Antenna *B*, reaching up to 4.11 GHz. The return loss of antenna revealed that it combined a number of wideband resonant frequencies, including those at 3.07 GHz, 3.90 GHz, 4.35 GHz, 5.15 GHz, and 6.32 GHz. The extra parasitic patches on the sheet positioned between the two substrates helped with this. There was also a 40 MHz-wide narrowband functioning between 1.15 GHz and 1.19 GHz, with resonance at 1.17 GHz.

Figure 6 shows the fabricated of Antenna *C* for measurement. Antenna *C* was made easier by the extracircular parasitic patches on the sheet sandwiched between the two substrates. The CPW and feedline were linked to this circular construction. Since this proposed antenna offers enormous bandwidth, less fading from multipath propagation, and low power consumption, wideband communication systems have recently attracted much interest.

A comparison of simulated and actual measured return loss of Antenna *C* is shown in Figure 7. The antenna had three primary resonances at 3.29 GHz, 5.51 GHz, and 6.67 GHz, with return losses of –24.678 dB, –17.654 dB, and –19.621 dB, respectively, and a 10 dB impedance bandwidth from 3.06 GHz to 7.0 GHz.

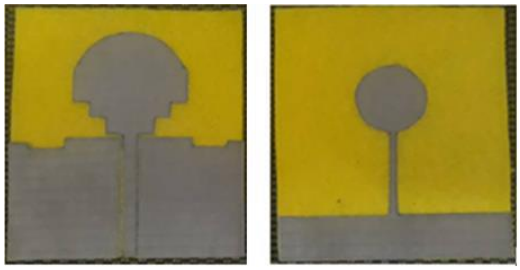

Fig .6. Fabricated of Antenna C for measurement

A comparison of Antenna *C*'s simulated and actual measured return loss is shown in Figure 7. The antenna had three primary resonances at 3.29 GHz, 5.51 GHz, and 6.67 GHz, with return losses of – 24.678 dB, – 17.654 dB, and – 19.621 dB, respectively, and a 10 dB impedance bandwidth from 3.06 GHz to 7.0 GHz.

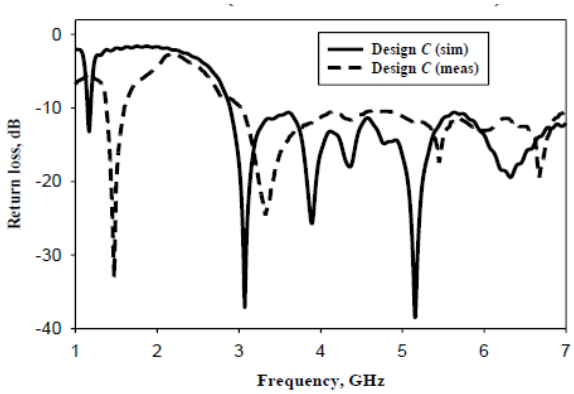

Fig .7. Return loss of Antenna *C* (Simulation and measurement)

Inconsistencies while fabricating with manual cutting tools, in addition to the uneven dielectric constant of substrate, are the main cause of the minor discrepancy between simulated and measured findings [21]. Since a perfect

connection is considered in simulations, the SMA connector losses in practice also have impact on the discrepancies between simulations and measurements. Apart from that, manner in which the epoxy is placed to galvanically link the SMA connection and fabric also has an impact on the amount of power supplied to the antenna during tests [22].

The simulated and tested effects deviated slightly at a few frequency points due to manufacturing flaws. The hand cutting of the textile material by using a manual cutter was the cause of this human error. The issue was also caused by fluctuations in the dielectric constant of constructed antenna, which varied depending on the ground location. The built-in antenna has a gain of 3.79 dB and 3.55 dB, respectively, for the simulation portions at 3.07 GHz and 5.15 GHz. The various performance results of Antenna *C* (simulation and measurement) are displayed in Table 3.

TABLE III. DIFFERENT PERFORMANCE RESULTS OF ANTENNA *C*

Ant	Resonant frequency, f_r (GHz)	Return loss (dB)	Bandwidth (GHz), $f_{High} - f_{Low}$ (GHz)	Gain (dB)	Dircv (dBi)
C (sim)	3.07	– 37.15	4.11, 2.89 – 7.00	3.79	7.42
	3.90	– 25.72		2.27	7.75
	4.35	– 18.03		2.74	7.83
	5.15	– 38.51		3.55	7.22
	6.32	– 19.43		5.51	9.21
C (meas)	1.47	– 33.54	0.19, 1.38 – 1.57	0.31	-
	3.29	– 24.67	3.94, 3.06 – 7.00	1.55	-
	5.51	– 17.65		2.15	-
	6.67	– 19.62		1.67	-

In Figure 8, the radiation pattern at = 0° and = 90° of Design C at two resonant frequencies (3.07 GHz and 5.15 GHz) showed a 0° direction with a tiny back lobe, and the same main direction was shown for the = 90° cut with two small back lobes oriented at 210° and 130°. The patterns at 5.15 GHz had a maximum in the 0° direction and a comparable form with the corresponding 0° and 90° cuts.

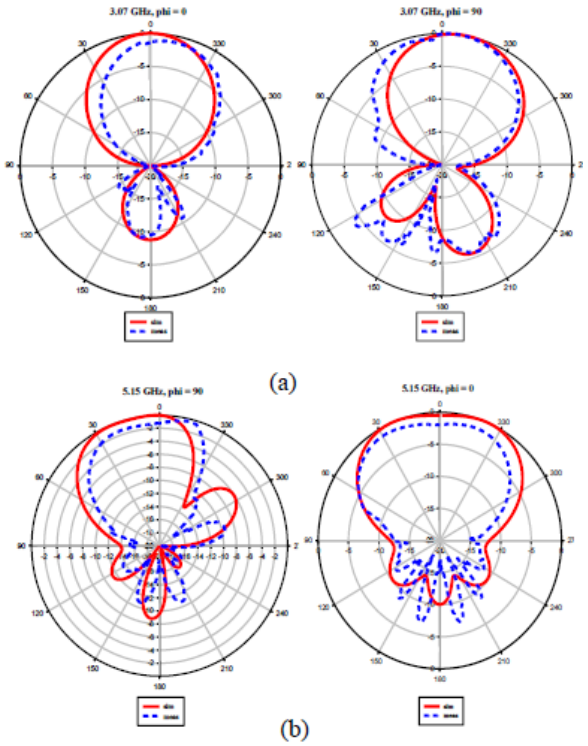

Fig. 8. Design *C*'s radiation pattern at 0° and 90° with two resonance frequencies of (a) 3.07 GHz and (b) 5.15 GHz

Figure 9 displays the predicted surface current of Antenna *C* at 0° and 90°. The surface current is a real electric current caused by an applied electromagnetic field. As illustrated in the picture, the current for Antenna *C* was based on three different locations: feedline, ground plane, and edge of the patch antenna (left and right sides). These two unique phases

(0° and 90°) demonstrated that the propagation fluxes of these two phases were virtually similar and balanced. It shows that the main highest flow are located at the at feedline, between the source to the patch.

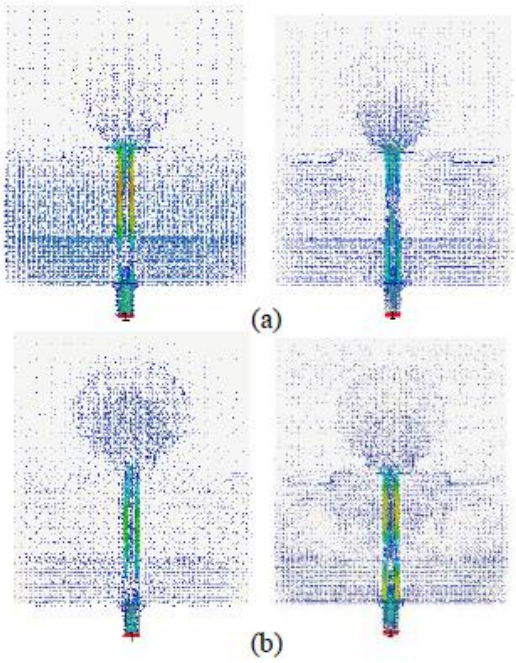

Fig. 9. Design *C*'s surface current at 0° and 90° with two resonance frequencies of (a) 3.07 GHz and (b) 5.15 GHz

CONCLUSION

It was claimed that antenna structure-based microwave breast imaging is the most promising for supplanting or enhancing the current gold standard of X-ray mammography in breast cancer diagnosis. In this research, a wideband, unidirectional antenna based on circular parasitic element approach was proposed with two layers of coplanar waveguide. The starting antenna design, Design *A*, worked at 3.94 GHz with a bandwidth of 3.83 GHz and a fractional bandwidth (FBW) of 97.2 %. It was followed by Design *B* which runs at 3.98 GHz with a bandwidth of 0.66 GHz and FBW of 56.53 %. The final Design *C* had a bandwidth of 4.11 GHz (79.8 %), centered at 5.15 GHz, and was intended to resonate at various frequencies between 2.89 GHz and 7.0 GHz for microwave imaging applications. Lastly, these proposed antenna design can be applied by other researchers to create a multifunction application future work system, especially on breast cancer detection.

ACKNOWLEDGMENT

The authors would like to thank Faculty of Electronics and Computer Engineering (FKEKK), Universiti Teknikal Malaysia Melaka (UTeM), Melaka, Malaysia for supportive work in obtained the information and material in the development for our work. Thanks to Centre for Research and Innovation Management of Universiti Teknikal Malaysia Melaka (CRIM-UTeM) and the Ministry of Higher Education (MoHE), Government of Malaysia.

REFERENCES

[1] Y. S., Faouri, S. Ahmad, N. O. Parchin, C. H. See, R. Abd-Alhameed, "A Novel Meander Bowtie-Shaped Antenna with Multi-Resonant and Rejection Bands for Modern 5G Communications,". Electronics, 11, 821, pp. 1-19, 2022

[2] Z. Guan, H. Yu, K. Cuk, Y. Zhang, H. Brenner, "Whole-Blood DNA Methylation Markers in Early Detection of Breast Cancer: A Systematic Literature Review," Cancer Epidemiology Biomarkers & Prevention, 28 (3), pp. 496-505, 2018.

[3] L. Wilkinson, T. Gathani, "Understanding breast cancer as a global health concern," The British Journal of Radiology, 95, 1130, pp. 1-3, 2022.

[4] H. Sung, J. Ferlay, R. L. Siegel, M. Laversanne, I. Soerjomataram, A. Jemal, "Global cancer statistics 2020: GLOBOCAN estimates of incidence and mortality worldwide for 36 cancers in 185 countries," CA: A Cancer Journal for Clinicians, 71: 209–49, 2021

[5] A. Janjic, M. Cayoren, I. Akduman, T. Yilmaz, E. Onemli, O. Bugdayci, M. E. Aribal, "SAFE: A Novel Microwave Imaging System Design for Breast Cancer Screening and Early Detection—Clinical Evaluation," Diagnostics. 11(3):533, pp. 1-10, 2021

[6] N. AlSawaftah, S. El-Abed, S. Dhou, A. Zakaria, "Microwave Imaging for Early Breast Cancer Detection: Current State, Challenges, and Future Directions," Journal of Imaging, 8 (5), pp. 1-31, 2022.

[7] S. Kwon, & S. Lee, "Recent Advances in Microwave Imaging for Breast Cancer Detection," International Journal of Biomedical Imaging, 5054912, pp. 1-26, 2016

[8] M. Fallahpour, "Synthetic aperture radar-based techniques and reconfigurable antenna design for microwave imaging of layered structures," Doctoral Dissertations, pp. 1-1847, 2013.

[9] M. D. Hossain, and A. S. Mohan, “Cancer Detection in Highly Dense Breasts Using Coherently Focused Time-Reversal Microwave Imaging,” IEEE Transactions on Computational Imaging, 3(4), pp. 928-939, 2017.

[10] M. Z. Mahmud, M. T. Islam, N. Misran, A. F. Almutairi, M. Cho, “Ultra-Wideband (UWB) Antenna Sensor Based Microwave Breast Imaging: A Review,”. Sensors. 18 (9) :2951, 2018

[11] X. Lin, Y. Chen, Z. Gong, Seet, B.C., Huang, L. and Lu, Y., 2020, “Ultra-Wideband Textile Antenna for Wearable Microwave Medical Imaging Applications” IEEE Transactions on Antennas and Propagation, pp. 1-1.

[12] M. N., Srifi, S. K., Podilchak, M. Essaaidi, and Y. M. M., Antar, “Planar circular disc monopole antennas using compact impedance matching networks for ultra-wideband (UWB) aplications,” APMC 2009 - Asia Pacific Microwave Conference, pp. 782-785, 2009

[13] N. A Jan, S. H. Kiani, D. A. Sehrai, M. R. Anjum, A. Iqbal, M. Abdullah, S. Kim, “Design of a Compact Monopole Antenna for UWB Applications,” Computers, Materials & Continua, 66 (1), pp. 35-44, 2021.

[14] A. Hossain, M. T. Islam, A. F. Almutairi, M. S. J. Singh, K. Mat, and M. Samsuzzaman, “An octagonal ring-shaped parasitic resonator based compact ultrawideband antenna for microwave imaging applications,”. Sensors, 20(5), pp.1-20, 2020.

[15] P. Cherian, T. A. Anjit, P. Mythili, “A Compact Egg - shaped UWB antenna for Breast Dielectric Profile Imaging,” International Journal of Scientific & Technology Research, 9(03), pp. 4672–4681, 2020

[16] A. Afyf, L. Bellarbi, A. Achour, F. Riouch, and A. Errachid, “A Novel Low Cost UWB Antenna for Early Breast Cancer Detection,” American Journal of Electromagnetics and Applications, 3(5), pp. 31-37, 2015

[17] A. Edalati, W. Shao, T. McCollough, and W. McCollough, 2017,” A Novel Cavity Backed Monopole Antenna with UWB Unidirectional Radiation,” Progress in Electromagnetics Research C, 72, pp. 1-13.

[18] Wang, F. and Arslan, T., “A thin-film-based wearable antenna array for breast microwave imaging and diagnosis,” First IEEE MTT-S International Microwave Bio Conference (IMBIOC), Gothenburg, pp. 1-4, 2017.

[19] H. Bahrani, E. Porter, A. Santorelli, B. Gosselin, M. Popovic, L.A Rusch, “Flexible 16 Antenna Array for Microwave Breast Cancer Detection,” IEEE Transactions on Biomedical Engineering, 62 (10), pp. 2516 – 2525, 2015.

[20] M. T. Islam, M. Samsuzzaman, M. Faruque, M. J. Singh, and M. Islam, “Microwave imaging based breast tumour detection using compact wide slotted UWB patch antenna,” Optoelectron. Advanced Materials Rapid Communications, 13, pp. 448-457, 2019.

[21] A. Mehdi, K. Abdennacer and S. Mounir, “Analysis of The Discrepancies Fabricating Error of Microstrip Antenna,” International Journal of Research and Reviews in Applied Sciences, 9 (3), pp. 405-412, 2011.

[22] K. Y. Yazdandoost and K. Sato, "Fabrication error in resonant frequency of microstrip antenna," Proceedings of 2001 International Symposium on Micromechatronics and Human Science (MHS2001), pp. 41-44, 200